DOI: 10.1002/((please add manuscript number))
Article type: Communication

Ultrafast all-optical switching of germanium-based flexible metaphotonic devices

*Wen Xiang Lim, Manukumara Manjappa, Yogesh Kumar Srivastava, Longqing Cong, Abhishek Kumar, Kevin F. MacDonald, and Ranjan Singh**

Wen Xiang Lim, Manukumara Manjappa, Yogesh Kumar Srivastava, Dr. Longqing Cong, Abhishek Kumar, Prof. Ranjan Singh
Division of Physics and Applied Physics, School of Physical and Mathematical Sciences, Nanyang Technological University, Singapore 637371, Singapore
Centre for Disruptive Photonic Technologies, The Photonics Institute, Nanyang Technological University, 50 Nanyang Avenue, Singapore 639798
E-mail: ranjans@ntu.edu.sg

Dr. Kevin F. MacDonald
Optoelectronics Research Centre and Centre for Photonic Metamaterials, University of Southampton, Southampton, SO17 1BJ, United Kingdom

Keywords: Ultrafast photoswitching, flexible metamaterial device, germanium, terahertz modulation

Abstract: Incorporating semiconductors as active media into metamaterials offers opportunities for a wide range of dynamically switchable/tunable, technologically relevant optical functionalities enabled by strong, resonant light-matter interactions within the semiconductor. Here, we experimentally demonstrate a flexible germanium (Ge) thin film-based metaphotonic device for ultrafast optical switching of terahertz (THz) radiation. A resonant transmission modulation depth of ~90% is achieved, with an ultrafast total recovery time of ~17 ps. A sub-picosecond decay constant of ~670 fs is obtained which is attributed to the presence of trap-assisted recombination sites in the thermally evaporated germanium film.

With the emergence of metamaterials,[1] it has become possible for electromagnetic waves to manifest extraordinary phenomena that are not possible in naturally occurring materials. Metamaterials are periodic structures of artificial 'meta-atoms', which have optical properties that are determined by the arrangement, size and shape of these atoms, enabling them to exhibit enhanced and unusual optical properties 'by design'. Plasmonic split ring resonators (SRRs) have been extensively studied as basic meta-atom building blocks for metamaterials, across the entire spectrum from microwave to optical frequencies, because they have the ability to interact with both the electric and/or magnetic field of incident electromagnetic waves.[1] Indeed, in the terahertz regime most of all they offer a means to supplement the extremely limited range of naturally occurring terahertz materials.[2-5] By breaking the symmetry of SRRs, the non-radiative mode of the plasmonic system can be excited and this manifests itself as a Fano resonance.[6-9] Such resonances can exhibit high quality factors and strong electric field confinement suitable for various applications such as lasing spasers,[10] bio-sensors,[11, 12] and slow-light devices.[13] The high sensitivity of Fano resonances to changes in the resonators' local (electromagnetic near-field) environment also greatly favours their utilization in switchable and reconfigurable metamaterial devices.[14] Dynamic modulation of the local environment is often achieved by hybridizing the plasmonic structure with a dielectric medium such as a semiconductor[15-25], chalcogenide or other phase-change media[26-28,29] with relative permittivities that can be reversibly manipulated via external stimuli such as heat[28-31], light[15-24, 27, 32] or voltage bias[25, 33]. In terms of practicality and technological relevance, semiconductors (in which free carriers may be excited optically) are highly desirable, particularly in regard to integration with current microelectronic and optoelectronic device technology platforms.

Silicon[15-19] and gallium arsenide[20-25] have been exploited in a variety of photonic metamaterial device structures, but germanium (Ge) as an indirect band gap semiconductor also holds considerable potential – it has a fundamental energy band gap (0.66 eV) which lies 0.14 eV below the direct band gap, large intrinsic carrier concentrations and high carrier mobilities, as compared to silicon. To fully exploit the rich optical properties of Ge, several schemes to lower the indirect band gap of Ge have been introduced which include modifying the material composition[34, 35], doping[36] and strain engineering.[37] Particularly, strain engineering promotes the formation of population inversion and increases inter-band radiative recombination at the lowered indirect band gap, hence Ge is also a suitable candidate as an optical gain medium.[38] The integration of Ge into Si-based material platforms has enabled a wide range of mid-IR photonic devices such as low loss waveguide and modulators.[39] A GeSi waveguide-based modulator operating at ultralow energy consumption was demonstrated with 0.2% of tensile strain.[40] An electrically pumped laser has been realized with tensile strain and *n*-doping of Ge such that direct recombination of electrons and holes occurs for lasing emission.[41] Ge also has the added advantage of CMOS compatibility in microelectronics.[42] Even in ultrathin films, Ge presents a high absorption coefficient, which has seen it employed in photonic devices such as solar cells[43] and photodetectors.[44, 45] The ultrafast carrier dynamics of crystalline Ge are particularly interesting, with recent studies reported using ultra-broadband mid-infrared spectroscopy[46] and ultrafast transient absorption spectroscopy[47] to probe the fast relaxation of photoexcited carriers. However, till date, there have been no demonstration of ultrafast Ge thin film metaphotonic devices.

In previous design of switchable devices, ultrafast photoswitching of LC resonances in metamaterials was attained on ErAs/GaAs superlattices.[20, 23] Superlattice structures possess periodic structures of two or more materials with large variation in their band gaps but similar lattice constant. In superlattices, lattice matching is crucial for short carrier lifetimes. In addition, the fabrication of superlattice requires alternating between two or more materials which is a complicated process as many growth factors have to be taken into consideration. In the previous demonstrations of photoswitching on GaAs[24] and other semiconductors (Si on Sapphire)[48], the recombination time of the carriers is >1 ns which indicates three orders of magnitude slower switching time compared to our results. Here we demonstrate, and explore the response dynamics, of thin film amorphous Ge as an active medium for ultrafast photo-induced switching of metamaterial resonances. Ultrafast photoswitching of Fano resonance is achieved by simply evaporating thin film Ge over the metamaterial array, which also allows us to achieve strong modulation of the Fano resonance. Contrary to superlattices, trap-assisted recombination sites due to structural defects in the non-crystalline Ge helps to boost the ultrafast carrier recombination. In addition, our fabrication is simple, cost-effective and involves thermal evaporation of a thin film single element semiconductor material. Lattice mismatch is not crucial in our design and the simplicity of the fabrication process makes it universally applicable to current state-of-the-art photonic devices. This could function as an ultrafast modulator or active filters. Our work could also pave the path for the realization of *flexible* electronic and photonic devices based on Ge.

In our study, a thin film of Ge is thermally evaporated onto the terahertz asymmetric split ring resonators (TASRs), which are fabricated on an ultrathin flexible Kapton film. An

optical pump beam excites free carriers in the Ge and shunts the capacitive gaps of the SRRs, thereby changing the THz transmission of the array. A sub-picosecond decay constant (~670 fs) is observed, which we attribute to the presence of structural defects in the non-crystalline Ge acting as trap-assisted recombination sites. The metaphotonic device structure provides ultrafast optically-induced modulation of THz transmission amplitude by up to ~90%.

A planar array of TASRs was fabricated using standard photolithography techniques on a 25 µm thick Kapton film substrate: A positive photoresist of thickness 1.5 µm was spin-coated onto the surface of the Kapton film and soft-baked at 105°C, making it photosensitive. It was exposed to high intensity UV light through a mask defining the TASR pattern (an array size of 1 cm × 1 cm) and exposed regions were then dissolved in a developer solution, uncovering the underlying Kapton (but leaving it otherwise unaffected). A 200 nm layer of aluminium was then thermally evaporated onto the substrate. The patterned photoresist layer (with its coating of aluminium) was then lifted off in an acetone solution, leaving the desired aluminium TASR metamaterial array on the Kapton substrate, as shown in **Figure 1a**. A 310 nm thick film of Ge was subsequently thermally evaporated onto the planar TASR array (Figure 1b). The dimensions of the TASR unit cell are annotated in Figure 1d: The square unit cell has a side length $p_{x,\,y}$ of 75 µm; the ASR side length s and width w are 60 µm and 6 µm, respectively; the capacitive gap size g is 3 µm – one of the gaps being at the midpoint of the top edge of the split ring, the other being on the bottom edge but offset by a distance x = 15 µm from the midpoint. The two arms of the split ring thus have different lengths, and we quantify the asymmetry of the design as the percentage ratio of the difference between 'left' and 'right' arm lengths (l_L and l_R) to the

total length of both arms: $\alpha = \frac{|l_L - l_R|}{|l_L + l_R|} \times 100\%$. In experiments, incident THz radiation is polarized in the *y*-direction, parallel to the unbroken sides of the TASRs (as indicated in Figure 1c), to excite the resonators' Fano resonance. As shown in Figure 1e, the evaporation of Ge onto the Fano resonators red-shifts the Fano and dipole resonances. This is attributed to the increase in the relative permittivity of the local environment surrounding the surface of the Fano resonators since the relative permittivity of Ge is higher than air.

As a control sample to the Ge-coated terahertz metaphotonic device, we first characterized the dynamic response of thermally evaporated Ge on Kapton in the absence of aluminium TASRs with a ZnTe crystal-based optical-pump/THz-probe (OPTP) spectroscopy. The output beam from an amplified Ti:sapphire laser producing optical pulses with an energy of 4 mJ and width of ~100 fs, at a centre wavelength of 800 nm (photon energy 1.55 eV) and a repetition rate of 1 kHz, is divided at a beam splitter; the transmitted beam pumps a ZnTe crystal to generate THz radiation with which the transmission of the sample is measured at normal incidence, while the reflected beam is used to optically excite the sample at oblique incidence, as illustrated in **Figure 2**. The diameters of the concentric THz and optical beam spots on the sample are respectively ~3 mm and ~10 mm, ensuring homogenous optical excitation of Ge over the area probed by the THz beam. The relative time delay between the terahertz and optical pulses was controlled by a delay stage. Fast Fourier transformation (FFT) of time-domain THz waveforms recover frequency-domain electric field spectra. Normalized transmission is then obtained as $T(\omega) = \frac{E_S(\omega)}{E_K(\omega)}$ where E_s and E_K are the electric field spectra of the sample and of the bare Kapton substrate respectively; ω being frequency.

Figure 3 shows the negative differential transmission $-\frac{\Delta T}{T_0}$ of Ge – the induced relative decrease in THz transmission (where $\Delta T = T - T_0$ is the absolute transmission change, T being the transmission at a given moment and T_0 that of the sample in the absence of optical excitation.) - as a function of the pump-probe time delay for a selection of average optical pump power levels. The magnitude of the induced change is maximized at a delay of 3 ps and increases linearly with pump power from 0.0314 at 200 mW (0.254 mJ/cm^2) to 0.1329 at 1200 mW (1.524 mJ/cm^2).

The dependence of $-\frac{\Delta T}{T_0}$ on pump power is consistent with the semiconductor to quasi-metal transition to which Ge is subject under optical excitation, which gives rise to an increase in photoconductive free carriers. The relative change in the transmission exhibits a characteristic exponential decay: mono-exponential decay profile convolved with the instrument response function is fitted to the experimentally measured data points in Figure 3, using the following equation:[49]

$$-\frac{\Delta T}{T} = e^{-\left(\frac{t-t_0}{IRF/2\ln 2}\right)^2} \times \left(A_0 + A_1 e^{\frac{t-t_0}{\tau_1}}\right) \quad (1)$$

where *IRF* is the full-width at half maximum of the instrument response function, A_0 is the constant and A_1 is the amplitude determining the weight of the exponential function, t_0 corresponds to time zero of the exponential fit and τ_1 is the decay time constant, values of which are found to increase as a function of pump power as given in Table 1, from 450 fs at 200 mW to 700 fs at 1200 mW. As photoexcited carriers relax from the conduction to the valence band, defect states present within the band act as trap-assisted recombination sites and become overpopulated by the large number of carriers relaxing. As a result, the number of available trap-assisted recombination sites decreases, leading to the increase in

decay time with pump power.[50] In our case, at 1200 mW (due to the limits of the laser power), the largest modulation of the differential transmission was attained and the corresponding decay time was ~700 fs. The sub-picosecond decay time validates Ge as a potential candidate for ultrafast photoswitching.

We subsequently investigated the response and relaxation dynamics of the Ge-functionalized TASR metamaterial array. In comparison to the bare Ge thin film, the maximum induced changes of the Ge functionalized on TASR metamaterial array occurs at a slightly longer time delay of 4.7 ps, which is due to the increase in the optical path length caused by the additional 200 nm thickness of aluminium metal resonator array. The magnitude of the light-induced transient change in THz transmission is enhanced in the metaphotonic device by around 70% relative to Ge on Kapton ($-\frac{\Delta T}{T_0}$ reaches a peak value of at 1200 mW of 0.2268 in the TASR metaphotonic structure as compared to 0.1329 for Ge alone). In keeping with the properties of Ge alone, the differential transmission of the metaphotonic device retains sub-picosecond decay time constants (670 ± 2 fs at 1200 mW, as illustrated in **Figure 4**). In addition, we observed similar complete carriers recombination lifetime for 100 nm and 310 nm thickness of Ge on Kapton substrate, which implies similar switching time (see details in Supporting Information, Figure S1).

The temporal evolution of the metaphotonic device's THz transmission spectrum is shown in **Figure 5a**. The time delay given in Figure 5a represents the relative time delay in the arrival of the pump (optical beam) and the terahertz probe at the sample position, which is controlled using the respective optical delay stages. For instance, time delay of 4.7 ps implies that the terahertz pulse arrives 4.7 ps after the arrival of the pump beam (800 nm)

at the sample surface. For each given time delay, the terahertz probe pulse is scanned subsequently through the sample and the substrate, which is converted into the frequency-domain using FFT. Between the time delay of -2.5 ps to 4.7 ps, the pump pulse impinges onto the sample and a large density of the carriers are photoexcited to the conduction band. At 4.7 ps, a sharp spike in the magnitude of the differential transmission occurs. Photoexcitation of carriers into the conduction band short-circuits the capacitive gaps of the split-ring resonators, resulting in the synchronous suppression of the Fano and dipole resonances, and thereby strong modulation of transmission, to maximum effect within 4.7 ps. As depicted in Figure 5b, the temporal evolution of the Fano resonance recovers more slowly than the dipole resonance (see details in Supporting Information, Figure S2). Unlike dipole resonance which is more insusceptible to changes in its local environment, Fano resonance is still moderately modulated by the presence of photoexcited carriers at a time delay of 7.3 ps. After which, relaxation of the photoexcited carriers restores the overall spectral response completely within ~17 ps.

Figure 6a shows the spectral dispersion of transmission at a pulse delay time of 4.7 ps: With increasing optical pump power, the TASR Fano resonance (characterized by a transmission dip at 0.75 THz and peak at 0.86 THz) is increasingly suppressed as the density of free carriers photoexcited into the conduction band increases. The trend towards saturation is clear, with the resonance being almost completely eliminated at an average pump power of 1200 mW, - the normalized resonance amplitude (inset to Figure 6d; defined as the difference between transmission levels at the THz peak and the THz dip of the Fano resonance, relative to the magnitude of this difference in the absence of optical excitation) is reduced at this point by ~90% as shown in Figure 6c.

This modulation of Ge-functionalized TASR metamaterial transmission resonance is elegantly reproduced in numerical simulations performed using the CST Microwave Studio package built in with a frequency domain solver based on the Finite Integral technique. In this model, the Kapton film and Ge are ascribed fixed real relative permittivities of 2.97 and 16, respectively and aluminium is modelled with a Drude conductivity of $\sigma = 3.56 \times 10^7\ S/m$; Periodic 'unit cell' boundary conditions were imposed in the *x*- and *y*- directions (i.e. in the sample plane); and incident plane wave THz radiation was taken to propagate in the *z*-direction with the electric field polarised in the *y*-direction as indicated in Figure 1c. The photoexcitation of Ge was modelled as an increase in its conductivity, as shown in Figure 6b, from 0 S/m (corresponding to zero optical pump intensity) to 9000 S/m - a level at which the change in resonant frequency THz transmission saturates, i.e. resonance amplitude falls to zero (indeed, the broad dipolar resonance upon which the TASR Fano resonance sits is also effectively suppressed at this conductivity level). To model the increase in the photoconductivity of the Ge with increasing pump powers, numerically fitted conductivity values (see details in Supporting Information, Figure S3) were used in the simulation model, and it correlates very well with the experimentally measured transmission amplitude, as shown in Figure 6b. As the conductivity values increase from 0 S/m to 9000 S/m, the transmission amplitude of the Fano and dipole resonance is slowly diminishing. Due to the photoconductive nature of Ge thin film overlayer on the entire metamaterial array, there is a strong synchronous modulation of both Fano and dipole resonances in the experimental results. As shown in **Figure 7**, there is strong confinement of electric field in the capacitive split gaps of the asymmetric resonators at the Fano resonance mode. When the sample is optically pump at 600 mW (0.762 mJ/cm^2), there is

a large reduction in the electric field confined within the split gaps. In the case of the highly sensitive Fano resonance, the switched-off response is clearly demonstrated before and after optical pump. However, the slight minor disparities between the zero-optical-pump experimental spectrum and the zero-conductivity simulated spectrum are attributed to manufacturing imperfections in the Al TASR array and defects in the Ge film that are not accounted for in the numerical model.

In summary, we have demonstrated the ultrafast photo-switching and THz transmission modulation characteristics of a metamaterial device comprising an aluminium asymmetric split ring array hybridized with a thin Ge film as an active medium. Resonant transmission is optically modulated on the picosecond time scale, with a sub-picosecond decay constant that is attributed to defects present in the amorphous Ge, which act as trap-assisted recombination sites for the relaxation of photoexcited free carriers. The operational (resonant) frequency of the device may be tuned by metamaterial design across a broad infrared to terahertz spectral range for a variety of applications in ultrafast microelectronic and optoelectronic devices, and in being fabricated on a Kapton film the structure has the added advantage of flexibility.

Supporting Information

Supporting Information is available from the Wiley Online Library or from the author.

Acknowledgement

This work is supported by research grants from Singapore Ministry of Education No. MOE2015-T2-2-103, and the Engineering and Physical Sciences Research Council, UK Grant No. EP/M009122/1.

Received: ((will be filled in by the editorial staff))
Revised: ((will be filled in by the editorial staff))
Published online: ((will be filled in by the editorial staff))

References:

[1] D. Smith, J. Pendry, M. Wiltshire, *Science* **2004**, *305*, 788.

[2] S. Linden, C. Enkrich, M. Wegener, J. Zhou, T. Koschny, C. M. Soukoulis, *Science* **2004**, *306*, 1351.

[3] H.-T. Chen, J. F. O'Hara, A. K. Azad, A. J. Taylor, *Laser Photonics Rev*. **2011**, *5*, 513.

[4] W. Withayachumnankul, D. Abbott, *IEEE Photonics J*. **2009**, *1*, 99.

[5] V. A. Fedotov, M. Rose, S. L. Prosvirnin, N. Papasimakis, N. I. Zheludev, *Phys. Rev. Lett.* **2007**, *99*, 147401.

[6] H.-T. Chen, J. F. O'Hara, A. K. Azad, A. J. Taylor, *Laser Photonics Rev.* **2011**, *5*, 513.

[7] B. S. Luk'yanchuk, N. I. Zheludev, S. A. Maier, N. J. Halas, P. Nordlander, H. Giessen, C. T. Chong, *Nat. Mater*. **2010**, *9*, 707.

[8] R. Singh, I. A. Al-Naib, M. Koch, W. Zhang, *Opt. Express* **2011**, *19*, 6312.

[9] R. Singh, I. Al-Naib, W. Cao, C. Rockstuhl, M. Koch, W. Zhang, *IEEE Trans. Terahertz Sci. Technol.* **2013**, *3*, 820.

[10] N. I. Zheludev, S. L. Prosvirnin, N. Papasimakis, V. A. Fedotov, *Nat. Photonics* **2008**, *2*, 351.

[11] A. A. Yanik, A. E. Cetin, M. Huang, A. Artar, S. H. Mousavi, A. Khanikaev, J. H. Connor, G. Shvets, H. Altug, *Proc. Natl. Acad. Sci. USA* **2011**, *108*, 11784.

[12] C. H. Wu, A. B. Khanikaev, R. Adato, N. Arju, A. A. Yanik, H. Altug, G. Shvets, *Nat. Mater.* **2012**, *11*, 69.

[13] N. Papasimakis, N. I. Zheludev, *Opt. Photonics News* **2009**, *20*, 22.

[14] K. Fan, W. J. Padilla, *Mater. Today* **2015**, *18*, 39.

[15] M. Manjappa, Y. K. Srivastava, L. Cong, I. Al-Naib, R. Singh, *Adv. Mater.* **2017**, *29*, 1603355

[16] K. Fan, A. C. Strikwerda, X. Zhang, R. D. Averitt, *Phys. Rev. B* **2013***, 87,* 161104.

[17] N. H. Shen, M. Kafesaki, T. Koschny, L. Zhang, E. N. Economou, C. M. Soukoulis, *Phys. Rev. B* **2009**, *79*, 161102.

[18] N.-H. Shen, M. Massaouti, M. Gokkavas, J.-M. Manceau, E. Ozbay, M. Kafesak, T. Koschny, S. Tzortzakis, C. M. Soukoulis, *Phys. Rev. Lett.* **2011***, 106,* 037403.

[19] H.-T. Chen, J. F. O'Hara, A. K. Azad, A. J. Taylor, R. D. Averitt, D. B Shrekenhamer, W. J. Padilla, *Nat. Photonics* **2008**, *2*, 295.

[20] H.-T. Chen, W. J. Padilla, J. M. O. Zide, S. R. Bank, A. C. Gossard, A. J. Taylor, R. D. Averitt, *Opt. Lett.* **2007**, *32*, 1620.

[21] K. Fan, X. Zhao, J. Zhang, K. Geng, G. R. Keiser, H. R. Seren, G. D. Metcalfe, M. Wraback, Z. Xin, R. D. Averitt, *IEEE Trans. Terahertz Sci. Technol.* **2013**, *3*, 702.

[22] M. R. Shcherbakov, S. Liu, V. V. Zubyuk, A. Vaskin, P. P. Vabishchevich, G. Keeler, T. Pertsch, T. V. Dolgova, I. Staude, I. Brener, A. A. Fedyanin, *Nat. Commun.* **2017**, *8*, 17.

[23] A.K. Azad, H.T. Chen, S.R. Kasarla, A.J. Taylor, Z. Tian, X.C. Lu, W. Zhang, H. Lu, A.C. Gossard, and J.F. O'Hara, *Appl. Phys. Lett.* **2009**, *95*, 011105.

[24] W.J. Padilla, A.J. Taylor, C. Highstrete, M. Lee, and R.D. Averitt, *Phys. Rev. Lett.* **2006**, *96*, 107401.

[25] H.T. Chen, W.J. Padilla, J.M.O. Zide, A.C. Gossard, A.J. Taylor, and R.D. Averitt, *Nature* **2006**, *444*, 597.

[26] Z. L. Samson, K. F. MacDonald, F. D. Angelis, B. Gholipour, K. Knight, C. C. Huang, E. D. Fabrizio, D. W. Hewak, N. I. Zheludev, *Appl. Phys. Lett.* **2010**, *96*, 143105.

[27] B. Gholipour, J. Zhang, K. F. MacDonald, D. W. Hewak, N. I. Zheludev, *Adv. Mater.* **2013**, *25*, 3050.

[28] C. Kodama and R. Coutu, Jr., *Appl. Phys. Lett.* **2016**, *108*, 231901.

[29] T. Driscoll, S. Palit, M. M. Qazilbash, M. Brehm, F. Keilmann, B. G. Chae, S. J. Yun, H. T. Kim, S. Y. Cho, N. M. Jokerst, D. R. Smith, D. N. Basov, *Appl. Phys. Lett.* **2008**, *93*, 024101.

[30] H. Tao, A. C. Strikwerda, K. Fan, W. J. Padilla, X. Zhang, R. Averitt, *Phys. Rev. Lett.* **2009**, *103*, 147401.

[31] R. Singh, A. K. Azad, Q. X Jia, A. J. Taylor, H.-Tong Chen, *Opt. Lett.* **2011**, *36*, 1230.

[32] M. Manjappa, Y. K. Srivastava, A. Solanki, A. Kumar, T. C. Sum, R. Singh, *Adv. Mater.* **2017**, 1605881

[33] W.-S. Chang, J. B. Lassiter, P. Swanglap, H. Sobhani, S. Khatua, P. Nordlander, N. J. Halas, S. Link, *Nano Lett.* **2012**, *12*, 4977.

[34] P. Moontragoon, Z. Ikonić, and P. Harrison, *Semicond. Sci. Technol.* **2007**, *22*, 742.

[35] S. Gupta, B. Magyari-Köpe, Y. Nishi, and K. C. Saraswat, *J. Appl. Phys.* **2013**, *113*, 073707.

[36] S. Prucnal, F. Liu, M. Voelskow, L, Vines, L. Rebohle, D. Lang, Y. Berencén, S. Andric, R. Boettger, M. Helm, S. Zhou, W. Skorupa, *Sci. Rep.* **2016**, *6*, 27643.

[37] C. Boztug, J. R. Sánchez-Pérez, F. Cavallo, M. G. Lagally, R. Paiella, *ACS Nano* **2014**, *8*, 3136.

[38] J. Liu, X. Sun, Y. Bai, K. E. Lee, E. A. Fitzgerald, L. C. Kimerling, and J. Michel, *Chin. Opt. Lett.* **2009**, *7*, 271.

[39] G. Z. Mashanovich, C. J. Mitchell, J. Soler Penades, A. Z. Khokhar, C. G. Littlejohns, W. Cao, Z. Qu, S. Stanković, F. Y. Gardes, T. Ben Masaud, H. M. H. Chong, V. Mittal, G. S. Murugan, J. S. Wilkinson, A. C. Peacock, and M. Nedeljkovic, *J. Lightwave Technol.* **2014**, *35*, 624.

[40] J. Liu, M. Beals, A. Pomerene, S. Bernardis, R. Sun, J. Cheng, L. C. Kimerling, J. Michel, *Nat. Photonics* **2008**, *2*, 433.

[41] R. E. Camacho-Aguilera, Y. Cai, N. Patel, J. T. Bessette, M. Romagnoli, L. C. Kimerling, J. Michel, *Opt. Express* **2012**, *20*, 11316.

[42] R. Pillarisetty, *Nature* **2011**, *479*, 324.

[43] V. Steenhoff, M. Theuring, M. Vehse, K. von Maydell, C. Agert, *Adv. Opt. Mater.* **2015**, *3*, 182.

[44] S. Assefa, F. Xia, Y. A. Vlasov, *Nature* **2010**, *464*, 80.

[45] Z. Xia, H. Song, M. Kim, M. Zhou, T.-H. Chang, D. Liu, X. Yin, K. Xiong, H. Mi, X. Wang, F. Xia, Z. Yu, Z. (J). Ma, Q. Gan, *Sci. Adv.* **2017**, *3*, e1602783.

[46] T.-T. Yeh, H. Shirai, C.-M. Tu, T. Fuji, T. Kobayashi, C.-W. Luo, *Sci. Rep.* **2017**, *7*, 40492.

[47] M. Zürch, H.-T. Chang, L. J. Borja, P. M. Kraus, S. K. Cushing, A. Gandman, C. J. Kaplan, M. H. Oh, J. S. Prell, D. Prendergast, C. D. Pemmaraju, D. M. Neumark, S. R. Leone, *Nat. Commun.* **2017**, *8*, 15734.

[48] J. Gu, R. Singh, X. Liu, X. Zhang, Y. Ma, S. Zhang, S. A. Maier, Z. Tian, A. K. Azad, H. Chen, A. J. Taylor, J. Han, and W. Zhang, *Nature Commun.* **2012**, *3*, 1151.

[49] M. ElKabbash, A. R. Rashed, B. Kucukoz, Q. Nguyen, A. Karatay, G. Yaglioglu, E. Ozbay, H. Caglayan, G. Strangi, *Nanoscale* **2017**, *9*, 6558.

[50] Y. Shi, Q.-L. Zhou, C. Zhang, B. Jin, *Appl. Phys. Lett.* **2008**, *93*, 121115.

Figure captions:

Figure 1. Optical microscope images of aluminium TASRs fabricated on a Kapton film **(a)** before and **(b)** after thermal evaporation of a 310 nm thick Ge coating. **(c, d)** Corresponding single unit cell images with the polarization of incident electric and magnetic fields illustrated in the former and the design dimensions of the TASR annotated in the latter. **(e)** Experimental results of the transmission spectra as a function of frequency for the aluminium TASRs metaphotonic device with and without the Ge.

Figure 2. Schematic illustration of the flexible aluminium TASR/germanium metaphotonic device under the OPTP spectroscopy. The planar TASR array was excited by an optical pump pulse and probe by a THz pulse.

Figure 3. Negative differential transmission $-\frac{\Delta T}{T_0}$ measured at the peak of THz time-domain pulse signal as a function of optical-pump THz-probe pulse delay for a 310 nm thick thermally evaporated Ge film on Kapton at a selection of average optical pump powers [as labelled]. Experimentally measured data points are fitted with mono-exponential decay profiles convolved with the instrument response function; plots are vertically offset from each other for clarity [in all cases $-\frac{\Delta T}{T_0}$ is zero at delay times <0 ps, and returns to zero within <15 ps after excitation].

Figure 4. Ultrafast response and relaxation dynamics of an aluminium TASR/germanium metaphotonic device. Negative differential transmission $-\frac{\Delta T}{T_0}$ at the peak of THz time-domain pulse signal as a function of optical-pump THz-probe pulse delay for an array of TASRs [on Kapton] coated with 310 nm of thermally evaporated Ge at an average pump powers of 1200 mW. Experimentally measured data points are with a mono-exponential decay fitting as per Eq. 1.

Figure 5. (a) Experimental results of the transmission spectra as a function of frequency at various time delay to illustrate the ultrafast photoswitching behaviour of the Ge-coated metaphotonic device. **(b)** The intensity plot maps the entire ultrafast on-off photoswitching of the Fano and dipole resonances which took ~17 ps [The resolution of the time delay is approximately 160 fs, calculated from the step size (25 μm) of the optical delay stage in the pump-probe path].

Figure 6. (a) Spectral dispersion of THz transmission for the Ge-coated TASR metaphotonic device at a selection of average optical pump power [as labelled], at a fixed pump-probe time delay setting of ~4.7 ps for which the transient optically-induced change in THz transmission is maximized [as shown in Figure 4]. **(b)** Corresponding numerically simulated spectra, whereby photoexcitation of Ge at increasing optical power levels is represented by increasing levels of conductivity. Normalized resonance amplitude evaluated from the transmission spectra of **(c)** experimental and **(d)** simulation results (the inset shows the evaluation of resonance amplitude).

Figure 7. Simulated electric field distributions of the Fano and dipole resonances before and after optical excitation. The strong electric field confinement at the capacitive gaps is strongly suppressed for the Fano resonance after the sample is optically pumped with 600 mW (0.762 mJ/cm^2), whereas the dipole field shows a minimal change. The maximum electric field strengths (before and after pump) located at the gaps of the Fano resonance mode are 12.03e6 V/m and 4.039e6 V/m respectively, whereas the dipole resonance mode shows maximum electric field strengths of 5.032e6 V/m and 2.77e6 V/m respectively.

Figure. 1

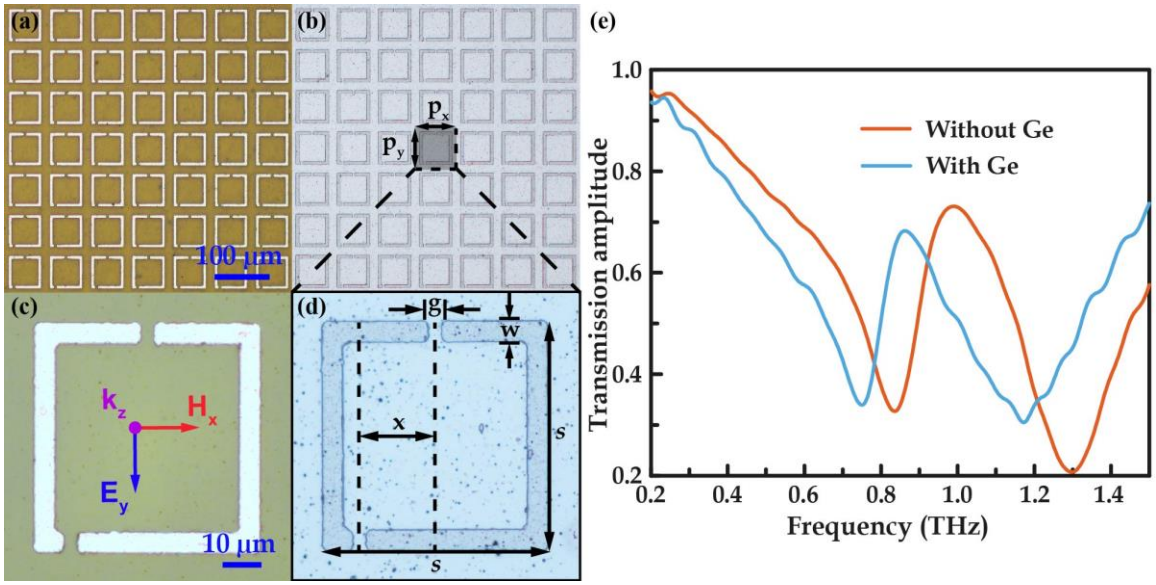
(a)
100 μm
(b)
p_x
p_y
(c)
k_z
H_x
E_y
10 μm
(d)
g
w
x
s
s
(e)
Without Ge
With Ge
Transmission amplitude
Frequency (THz)
1.0
0.8
0.6
0.4
0.2
0.2
0.4
0.6
0.8
1.0
1.2
1.4

Figure. 2

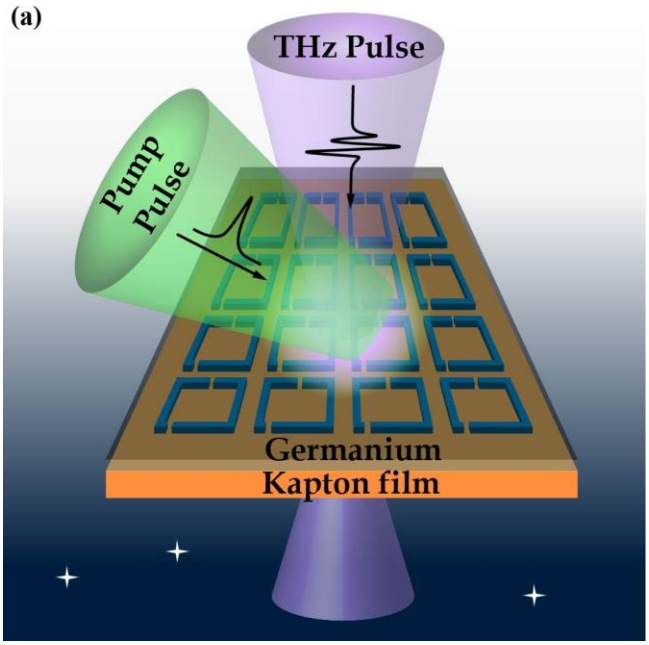

Figure. 3

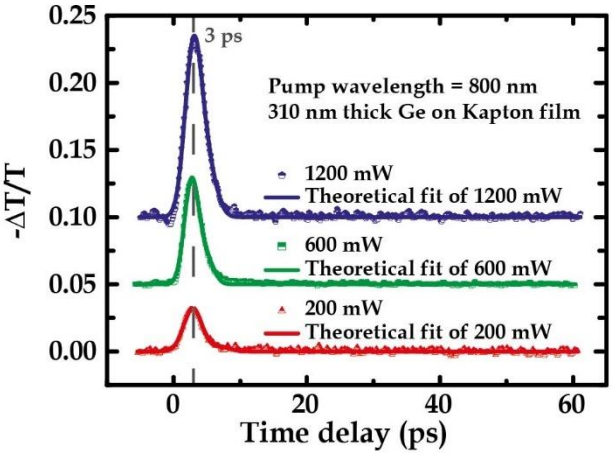
0.25
0.20
0.15
0.10
0.05
0.00
-ΔT/T
3 ps
Pump wavelength = 800 nm
310 nm thick Ge on Kapton film
1200 mW
Theoretical fit of 1200 mW
600 mW
Theoretical fit of 600 mW
200 mW
Theoretical fit of 200 mW
0
20
40
60
Time delay (ps)

Figure. 4

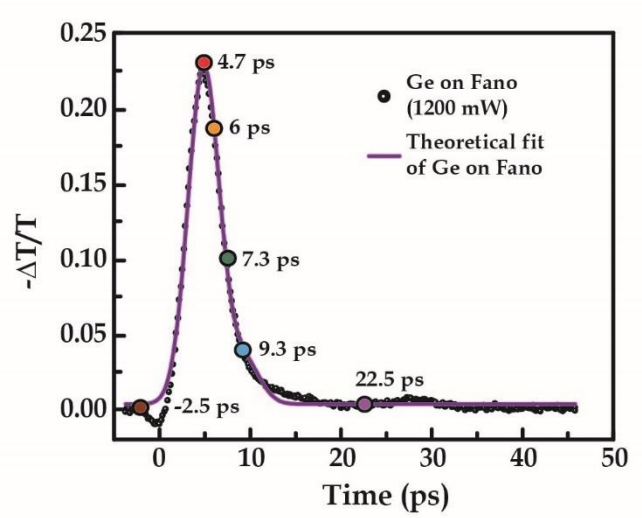
0.25
0.20
0.15
0.10
0.05
0.00
-ΔT/T
0
10
20
30
40
50
Time (ps)
4.7 ps
6 ps
7.3 ps
9.3 ps
22.5 ps
-2.5 ps
Ge on Fano
(1200 mW)
Theoretical fit
of Ge on Fano

Figure. 5

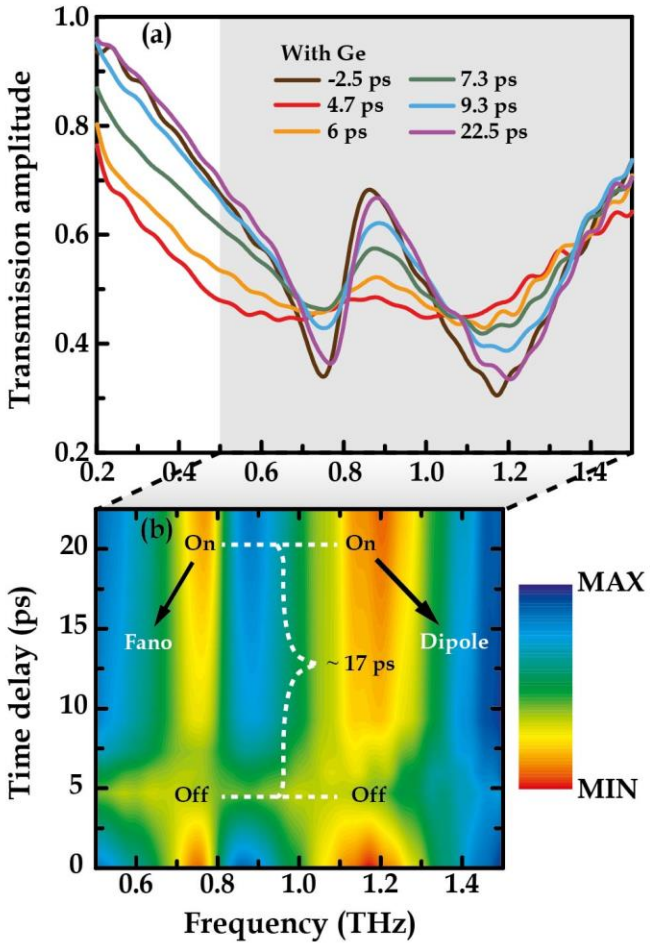
(a)
With Ge
-2.5 ps
4.7 ps
6 ps
7.3 ps
9.3 ps
22.5 ps
Transmission amplitude
1.0
0.8
0.6
0.4
0.2
0.2
0.4
0.6
0.8
1.0
1.2
1.4
(b)
On
On
Fano
Dipole
~ 17 ps
Off
Off
MAX
MIN
Time delay (ps)
20
15
10
5
0
0.6
0.8
1.0
1.2
1.4
Frequency (THz)

Figure. 6

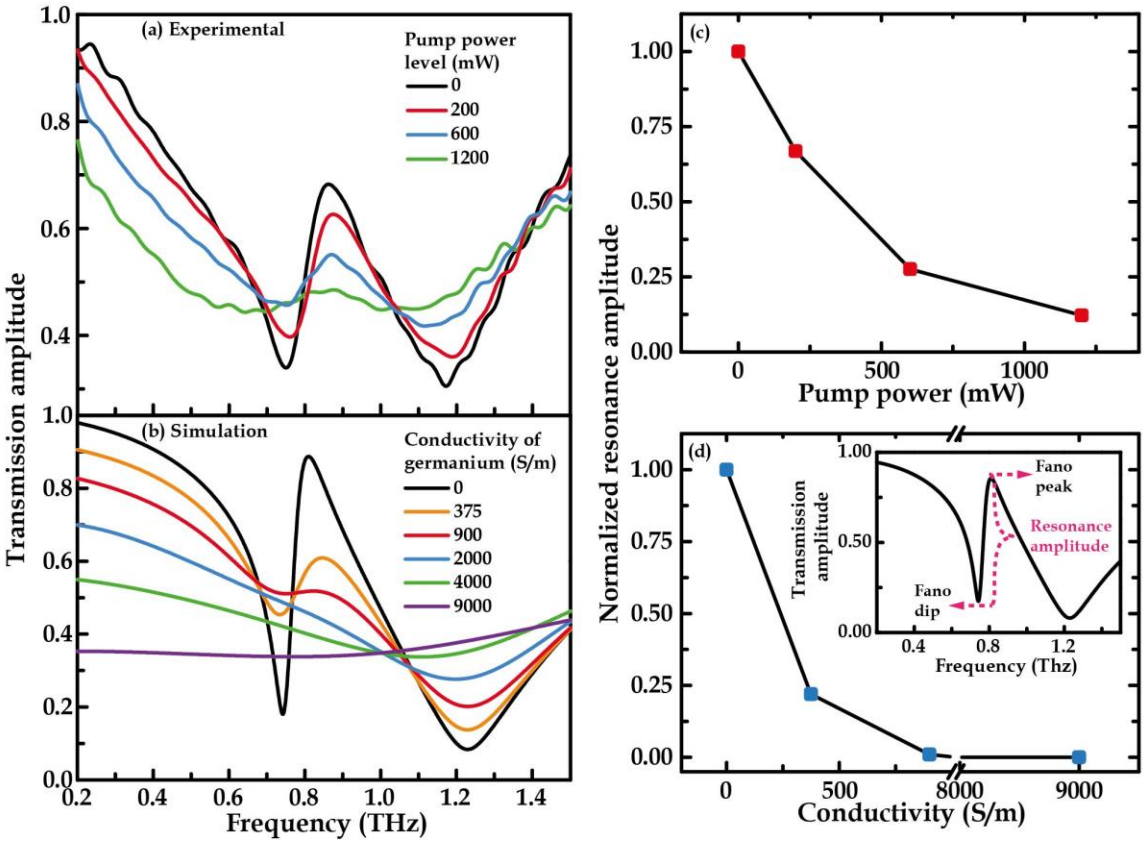
(a) Experimental
Pump power level (mW)
0
200
600
1200
(b) Simulation
Conductivity of germanium (S/m)
0
375
900
2000
4000
9000
Transmission amplitude
Frequency (THz)
(c)
Normalized resonance amplitude
Pump power (mW)
(d)
Transmission amplitude
Fano peak
Resonance amplitude
Fano dip
Frequency (Thz)
Conductivity (S/m)

Figure. 7

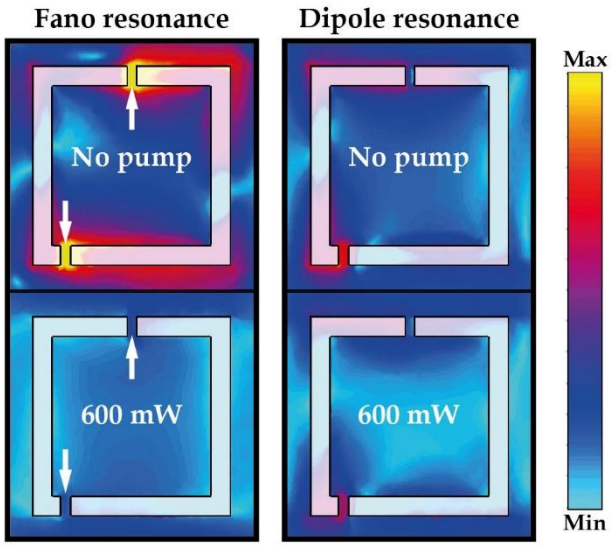
Fano resonance
Dipole resonance
No pump
No pump
600 mW
600 mW
Max
Min

Table caption:

Table. 1 Exponential decay time constants for the optically-induced change in THz transmission of thermally evaporated Ge at a selection of pump power levels derived from mono-exponential fittings (Eq. 1) to the dependences of negative differential transmission on pump-probe pulse delay shown in Figure 3.

Table. 1

Pump power (mW)	**200**	**600**	**1200**
τ_1 (fs)	450 ± 2	520 ± 1	700 ± 2

Supporting Information

Ultrafast all-optical switching of germanium-based flexible metaphotonic devices

*Wen Xiang Lim, Manukumara Manjappa, Yogesh Kumar Srivastava, Longqing Cong, Abhishek Kumar, Kevin F. MacDonald, and Ranjan Singh**

Thickness dependence of Ge thin film on switching behaviour

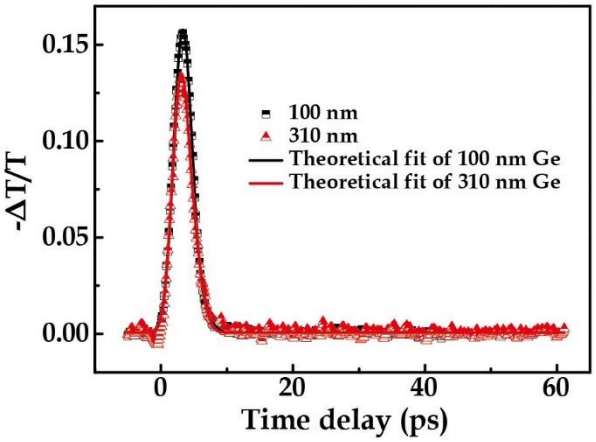

Figure S1. Measured and the theoretical fit of the ultrafast relaxation dynamics of Ge thin film with thickness of 100 nm and 310 nm.

As shown in Figure S1, OPTP measurement was performed using another sample with 100 nm Ge thin film on Kapton substrate and compared with our current results. By comparing the relaxation dynamics of Ge thin film of different thicknesses, we obtained from the theoretical fit (using equation 1 of main text) a decay time constant of 540 ± 3 fs for the 100 nm thick Ge thin film which is faster than the 310 nm thick Ge thin film (700 ± 2 fs). However, the relaxation dynamics show similar complete carriers recombination for both

100 nm and 310 nm thickness of Ge on Kapton substrate, which implies similar switching time.

Temporal evolution of Fano and dipole resonances

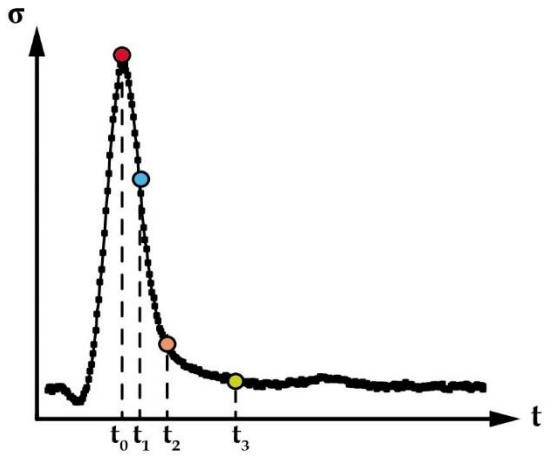

Figure S2. Schematic of the relaxation dynamics of Ge on Fano resonators

Fano resonance recovers slower than the dipole resonance because of the highly sensitive nature of the resonant electric field (at Fano resonance frequency) tightly confined in the capacitive split gaps of the asymmetric resonators. Fano resonance is a sharp narrow linewidth resonance mode that results from the destructive interference between the bright and the dark mode. Slight perturbations in the immediate environment or geometry of the metamaterial system dramatically affects the linewidth, strength or frequency of the Fano resonance. However, dipole resonance is a broad linewidth fundamental mode of the perfectly symmetric resonator system and requires stronger changes to its local environment before it can be disturbed. The field distributions at both the resonance modes can be observed (in Figure 7 of main text) which clearly show a strong field confinement for the Fano mode than for the dipole mode. Thus, when 310 nm of Ge thin-film overlayer

is coated on top of the metasurface and then the pump photoexcitation beam is switched on, the resonant fields at Fano and dipole undergoes a modulation. Since the intense Fano resonant electric fields are tightly confined in a small spatial volume of the capacitive split gaps of the asymmetric resonators, small increase in the conductivity of the Ge thin-film causes large modulation (switch-off) of the Fano resonance. Therefore, the Fano resonance fails to recover completely until almost all photo-excited carriers have relaxed to the equilibrium state. On the other hand, the field distribution and intensity at the dipole resonance is neither as confined nor so intense in comparison to the Fano fields. Therefore, small enhancement in Ge photoconductivity does not lead to a large modulation (switch-off) of the dipolar resonance. In fact, we observe a scenario where the dipole resonance survives even for large enhancement in Ge photoconductivity, thus leading to a faster recovery of the dipole resonance well before all the photo-excited carriers relax back to the equilibrium state. We further explain this phenomena in detail with respect to the relaxation dynamics at different time instants in Figure S2 below:

With the different field distributions of Fano and dipole resonances, they exhibit different dependence on the photoconductivities of Ge thin film. At t_0, majority of the free carriers are photoexcited to the conduction band which is also the peak photoconductivity of Ge. At this point, it reflects the quasi-metallic state of the Ge. As a result, both Fano and dipole resonances are strongly modulated. During the initial photo-carrier relaxation process, the dipole resonance possessing the higher photoconductivity threshold reappears faster (at t_1), while the evolution of the Fano resonance will be slower till the threshold photoconductivity for the Fano resonance is reached. At t_2, the number density threshold point for the Fano resonance is reached and the resonance starts to recover. Thereafter, at

t_3, there is complete relaxation of the photoexcited carriers and Ge loses majority of its conductivity. Therefore, both resonances recover their overall spectral response.

Photoconductivity extracted at different pump powers

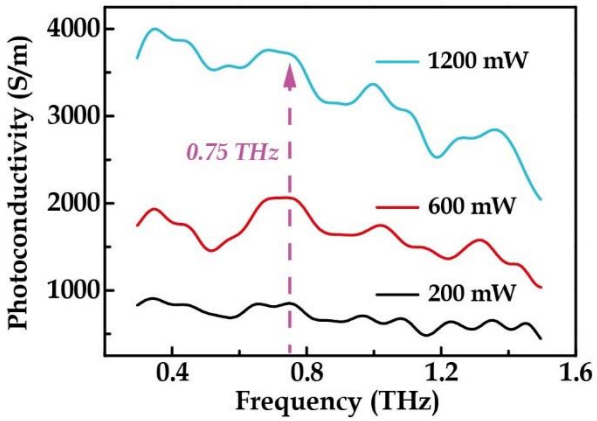

Figure S3. Extracted photoconductivity values by measuring the terahertz transmission through 310 nm of Ge thin-film on bare Kapton substrate as a function of frequency at a selection of average optical pump powers.

The transmission spectrum of bare Ge film on Kapton substrate without metamaterial was measured at different average optical pump powers. The photoconductivity of thin film Ge corresponding to optical pump powers of 200 mW (0.254 mJ/cm^2), 600 mW (0.762 mJ/cm^2) and 1200 mW (1.524 mJ/cm^2) were extracted using optical-pump/THz-probe (OPTP) spectroscopy as illustrated in Figure S3, where the thin Ge (310 nm thick) on Kapton substrate is photoexcited by 800 nm optical pump beam. The change in the differential transmission of terahertz pulse ($\frac{-\Delta T}{T}$) is directly proportional to the carrier densities and the photoconductivity. Hence, the change in photoconductivity can be evaluated by[1]

$$\Delta\sigma(\omega) = \frac{\varepsilon_0 c(n_{air} + n_{sub})}{d}\left[\frac{-\Delta T(\omega)}{T}\right]$$

where c is the speed of light, d is the thickness of Ge, n_{air} and n_{sub} are the refractive indices of air and substrate respectively. With an approximately non-dispersive property of the photoconductivity in the interested band, the photoconductivity values at Fano resonance frequency of 0.75 THz have been used in simulations to observe the modulation of Fano resonance.

Supporting References

[1] H. K. Nienhuys and V. Sundström, *Phys. Rev. B* **2005** *71*, 235110.